Three-Dimensional Simulation of Bulge Formation in Contact Hole Metalization

W. Pyka and S. Selberherr

Institute for Microelectronics, TU Vienna
Gusshausstrasse 27–29, A–1040 Vienna, pyka@iue.tuwien.ac.at

ABSTRACT

During sputter deposition of metal layers bulges at sharp convex corners can arise and are observed after metalization of contact holes for semiconductor circuits. We present an explanation of this phenomenon by assuming that in process steps prior to the deposition a ledge is formed. This assumption together with the choice of an appropriate model for the distribution of the incident particles explains the evolution of the resulting film profile including the bulge at the topmost convex corner of the structure. The profile is simulated for several positions on the wafer. The variation of bulge shape and film thickness depending on the orientation of the sidewalls for the peripheral positions is reproduced. We investigate the geometry and particle flux conditions and show simulation results for different geometries, contact hole diameters, aspect ratios and angles of incidence. Simulation results are compared with SEM pictures obtained from experiments.

Keywords: Topography Simulation, Bulge Formation, Sputter Deposition, Metalization, Titanium Nitride

INTRODUCTION

In current integrated circuits technology thin barrier layers are used to improve and to optimize the properties of contacts, vias and interconnect structures. The knowledge about film thicknesses which vary with process parameters and with the topography of the applied structures, and the achievement of good film conformality and step coverage are the most important tasks for choosing an appropriate deposition technique. Some Chemical Vapor Deposition (CVD) techniques are available at research and development level [1], but could not yet supersede the well established Physical Vapor Deposition (PVD) processes such as magnetron sputtering, which allow a reasonable throughput and a good control of the film stoichiometry. Approaches with collimated sputtering of titanium and titanium nitride films [2] improve bottom coverage, but are doubtful in sidewall coverage and questionable due to costs of consumable parts and particle contents. However, to overcome the drawback of worse conformality at extreme topographies with high aspect ratios arising from the line of sight type sputter deposition, it is necessary to carefully investigate the actual deposition techniques and extend them to the limit of their applicability.

Simulation of deposition processes gives a deeper insight into the geometry and particle distribution conditions. In this article we describe the deposition simulation of titanium nitride (TiN) layers. The simulations are performed for several contact hole diameters and aspect ratios. TiN is chosen because among other materials, it has been recognized as excellent barrier material and is used as nucleation/glue layer at the contact/via level as well as a diffusion barrier and anti-reflection coating in the interconnect stack [3]. We have calibrated an analytical distribution function to a specific reactor equipment and compared the simulation results with the experimental SEM pictures. Beyond the evolution of the overall film profile the SEM pictures showed the appearance of bulges at the uppermost convex edge of the circular shaped contact hole structures. We have assumed, that during preliminary processing of the contact holes (layer deposition, mask exposure, resist development and etching) a ledge is formed at the topmost edge which is responsible for the formation of the bulge during the exposition to the particle stream.

SIMULATION

For the simulation we use a structuring element algorithm derived from image processing [4]. The geometry is represented by a cellular structure and a material index is assigned to each cell. For each surface cell the visibility conditions according to the topography are determined and the deposition rate $\vec{v}_d$ is calculated by vector integration of a given distribution function $F(\vartheta)$ over the solid angle Ω visible for the actual position.

$$\vec{v}_d = \frac{R}{N} \int_{\Omega} F(\vartheta)\, \mathrm{d}\Omega \tag{1}$$

In this equation R is the macroscopic deposition rate determined by layer thickness at flat surfaces and deposition time and N is a normalizing factor

$$N = \int_{2\pi} F(\vartheta)\,\mathrm{d}\Omega\,, \tag{2}$$

which ensures that for a flat, unshadowed surface the integrated deposition rate equals the macroscopic deposition rate R. This results in an overall deposition vector with a length $|\vec{v}_d|$ representing the deposition rate and a direction which accounts for the averaged angle of incidence of the particles scattered in the plasma chamber. The direction of the deposition vector $\vec{v}_d$ represents the growth direction for the considered surface cell.

GEOMETRIC CONDITIONS FOR BULGE FORMATION

We assume that chemical mechanical polishing (CMP) or mask underetching during preliminary process steps leads to the formation of a ledge at the top corner. This results in a geometry as depicted in Figure 1. The cellular data format used for the simulation can be seen.

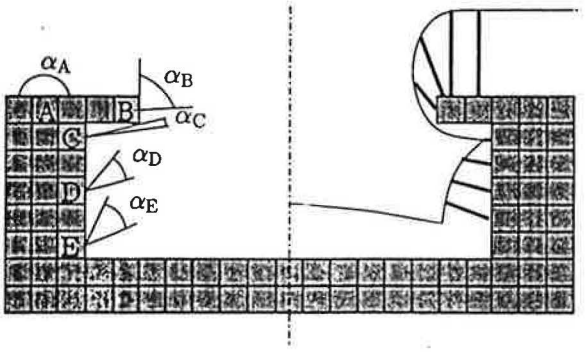

Figure 1: Visibility conditions, schematics of deposition rates and resulting profile at ledges.

When integrating the particle distribution function for the surface cells, the visibility limits are as follows. For cell A the whole upper hemisphere is visible. Thus the integrated deposition rate is the macroscopic rate R. At cell B the left half is shadowed. Therefore the deposition rate is half the rate of cell A (for the central symmetric case) and the main axis of the structuring element is inclined due to the vector integration of the contributing parts. The deposition rate at position C is almost zero because the sputter target is completely shadowed and only a small fraction of scattered particles may arrive at this position. Since towards position D the visible solid angle increases again, this effect gives rise to

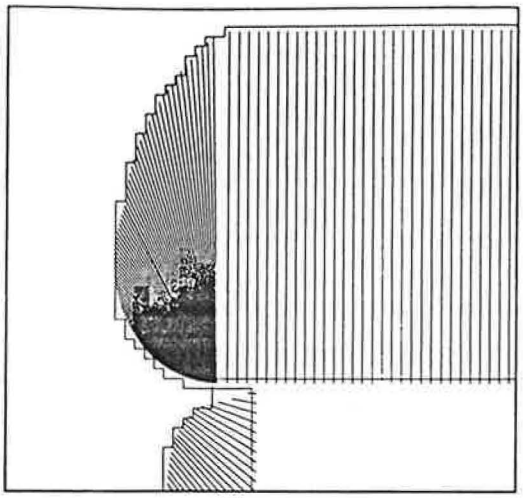

Figure 2: Calculated deposition rates and resulting cellular structure at a ledge. The depicted area is 0.3 μm × 0.3 μm wide.

the lower edge of the bulge. Depending on the distribution function and on the aspect ratio of the considered structure, the deposition rate reaches a maximum between positions D and E and again decreases towards the bottom of the hole.

Special care has to be taken for cell B to compensate for the abrupt change in the deposition rate. We calculate the deposition rate for rotated cells at position B for taking into account a microscopic curvature of the ledge. With each increment of the rotation angle a larger part of the source becomes shadowed and therefore the deposition rate decreases. If sufficiently many of such rotated cells are considered, the smooth shape of the bulge is reconstructed.

On the right hand side of Figure 1 a schematic of the size and the direction of the corresponding structuring elements and the resulting deposition profile are

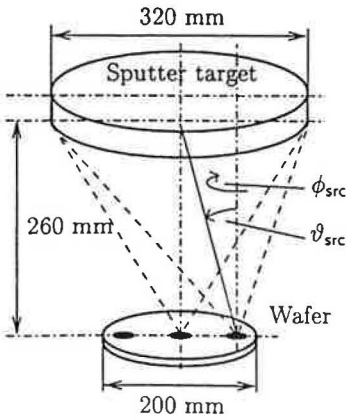

Figure 3: Experimental arrangement and location of the simulated structures.

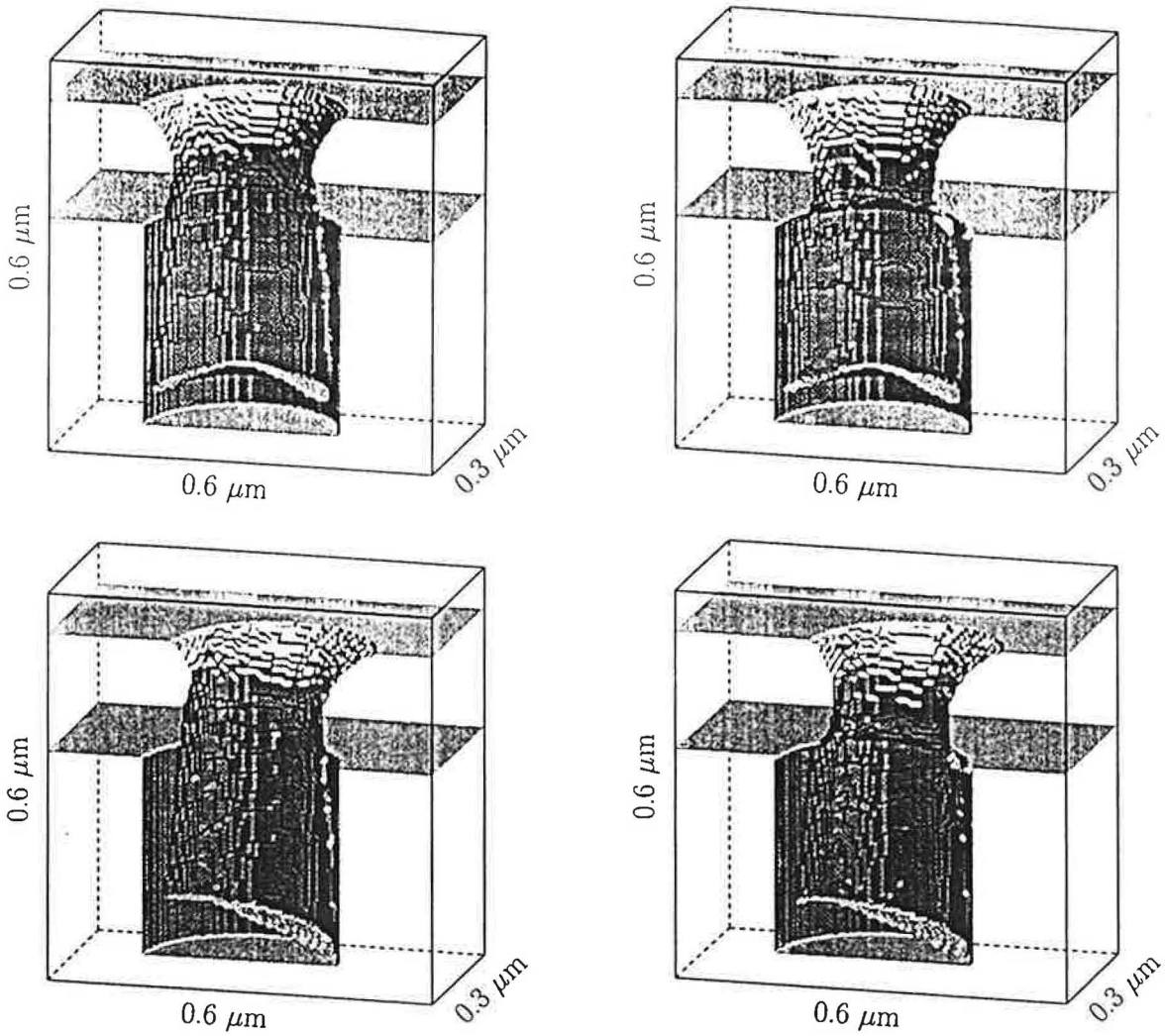

Figure 4: Deposition of TiN into a 0.3 μm diameter and 0.3 μm deep test structure. The deposition rate is 33.8 nm/min and the simulation time is 320 s. The pictures on the top show the resulting profile for a contact hole in the center of the wafer, the pictures at the bottom are simulated at a position 90 mm off the wafer center. For the images on the left no initial ledge is assumed and the resulting profiles on the convex corner are smooth. The input geometries on the right include an initial ledge at the topmost edge and show the formation of a bulge.

depicted. The evolution of the film profile at a ledge isolated from the complete structure for a center wafer position with a symmetric distribution function is demonstrated in Figure 2. For this example, the size of the edge is exaggerated to clearly illustrate the simulation model of the bulge generation. The deposition rate and the final cellular geometry are also visualized in Figure 2.

PARTICLE DISTRIBUTION MODEL

The most important factor for the resulting layer profile is modeling and calibration of the particle flux. We approximate the distribution of particles arriving at the wafer surface by fitting and calibrating a function to the angular distributions resulting from Monte Carlo simulations of sputtering particle transport [5]. The models used for the particle emission from the sputter target [6] [7] use fractal surface representations. The simulation principles of the particle transport within the plasma are quite general and therefore can also be applied to the titanium target in the argon-nitride plasma reactor. The analytical distribution function is an exponential function given by

$$F(\vartheta) = a\vartheta^3 e^{-b\vartheta}. \tag{3}$$

In addition a lateral component may be added which accounts for the slight difference of the flow conditions between the topmost edge and the bottom of the contact hole. This fraction impacts the overall profile evolution but only little influences the shape of the bulge.

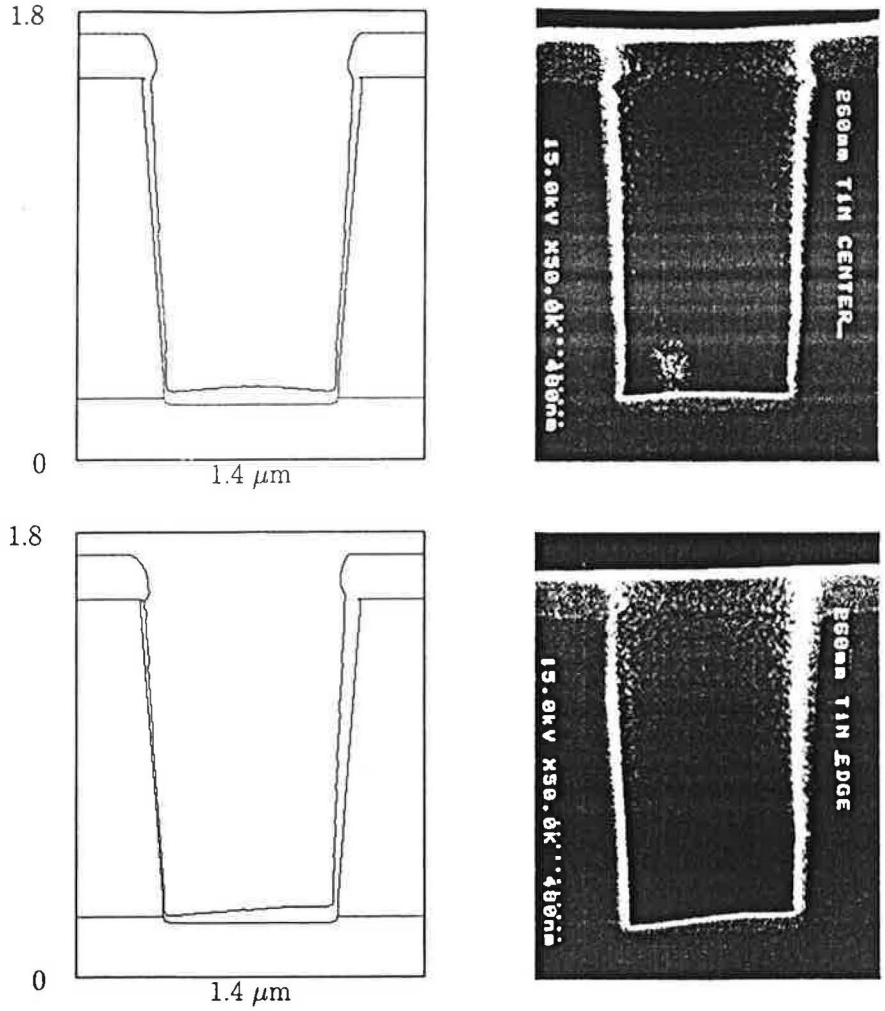

Figure 5: Deposition of TiN into a 0.7 μm diameter and 1.3 μm deep contact hole structure. The deposition rate is 33.8 nm/min and the simulation time is 320 s. The pictures on the top are for a center-wafer position, the pictures at the bottom for a position 90 mm off the wafer center. The pictures on the left show cross-sections through a three-dimensionally simulated structure, the corresponding SEM pictures are on the right.

The direction of maximum particle incidence and the amount and the gradient of the lateral fraction are adjustable. The parameters are internally converted to the constants used in the distribution function (3).

SLANTED PARTICLE INCIDENCE

Moreover, we simulate the deposition at several wafer positions by setting different polar and azimuthal angles of the source position as depicted in Figure 3.

The polar angle ϕ_{src} and the azimuthal angle ϑ_{src} determine the origin of the particle distribution function. Since the circular contact holes are radially symmetric, the simulation results are independent of ϕ_{src} but vary with ϑ_{src}, the angle between the connection line from the sputter target center to the considered wafer position and the vertical z-axis.

INPUT GEOMETRIES

We have performed simulations for different geometries. For calibration and testing issues we use a circular hole with 0.3 μm diameter and 0.3 μm depth. The sidewalls of these structures are exactly vertical. The structure is built with a solid modeling program based on the same cellular data representation as used for the topography simulation.

Furthermore the input geometry for a contact hole structure with 0.7 μm diameter and a depth of approximately 1.3 μm is extracted from SEM pictures and imitated with the solid modeling program. The structure consists of silicon dioxide on silicon with slanted sidewalls. The input geometry can be seen in the cross-sections of the simulation results in Figure 5.

TEST STRUCTURES

Figure 4 shows the results of the deposition simulation for a 0.3 μm diameter, 0.3 μm deep circular hole located 260 mm below the center of the sputter target disk. For the top left example at a position exactly below the center of the sputter target disk no initial ledge has been assumed. As expected, the resulting structure is axially symmetrical and no bulge appears.

Below, the deposition at a position 90 mm off the wafer center for the same geometry is performed by a 20° azimuthal offset of the distribution function. ϕ_{src} is set to 90° so that the center of the sputter target is right from the center of the structure. The asymmetric profile reflects the slanted angle of principle incidence. The left sidewall is oriented towards the target whereas for the right sidewall a much higher fraction of the incident particles is shadowed. This causes different film thicknesses depending on the orientation of the sidewall. For the geometries on the right an initial ledge is added to the input geometry. In this case a bulge is formed at the convex edge. For the center wafer position again it is radially symmetric whereas for the off-center location the shape of the bulge depends slightly on the polar orientation of the contact hole sidewall.

CONTACT HOLES

Finally, Figure 5 correlates simulation results of TiN-film deposition into a 0.7 μm diameter silicon-silicon-dioxide structure with experimental results.

Again the pictures on the top represent the center wafer position and the pictures below the location off the center. For this case ϕ_{src} is set to $-90°$, the sputter target is left from the structure. Two-dimensional cross-sections of three-dimensional simulations are related to the corresponding SEM pictures on the right. The simulation as well as the SEM pictures indicate the radially symmetric layer profile and bulge shape for the center wafer case. For the slanted direction of main particle incidence (depicted on the bottom of Figure 5) the conditions at the ledge are different depending on the exposition of the convex edge. The same as explained for the sidewall film thickness applies to the evolution of the shape of the bulge. The right edge faces towards the target center and therefore is strongly exposed to the particle flux mainly arriving with inclined incidence. The summarized deposition rate is higher and has a higher lateral component. Therefore a higher amount of material is deposited at the regions below the ledge and the bulge is not as pronounced as on the left edge side. Even if the deposition rate is smaller, the variation due to the shadowing effect of the ledge is higher. The resulting difference in the bulge shape is evident in Figure 5.

CONCLUSION

We have shown that by introducing a ledge, it is possible to explain and to simulate the formation of bulges at convex corners. If such phenomenons are undesirable within the process flow, special care has to be taken in preceding process steps. Obviously the simulation of the flow conditions within the plasma or measurements of the incoming particle distribution would be desirable, but the analytical particle distribution model and the model of arbitrary location of the sputter target by setting its position by the angles ϕ_{src} and ϑ_{src} are capable of reproducing the film profiles including bulges obtained from experimental investigations. The selected analytical function is a good representation of the particle incidence conditions at the wafer surface.

ACKNOLEDGEMENTS

This research project is supported by SONY Corporation Atsugi Technology Center, Atsugi. Japan, Austria Mikro Systeme International AG, Unterpremstätten, Austria and Christian Doppler Forschungsgesellschaft, Vienna, Austria.

REFERENCES

[1] C. Faltermeier, C. Goldberg, M. Jones, A. Upham, D. Manger, G. Peterson, J. Lau, A. E. Kaloyeros, B. Arkles, and A. Paranjpe, "Barrier Properties of Titanium Nitride Films Grown by Low Temperature Chemical Vapor Deposition from Titanium Tetraiodide," *J.Electrochem.Soc.*, 144, 3, 1002–1008, 1997.

[2] J. G. Ryan, S. B. Brodsky, T. Katata, M. Honda, N. Shoda, and H. Aochi, "Collimated sputtering of Titanium and Titanium Nitride Films," *MRS Bulletin*, 20, 11, 42–45, 1995.

[3] M. Eizenberg, "Chemical Vapor Deposition of TiN for Sub-0.5 μm ULSI Circuits," *MRS Bulletin*, 20, 11, 38–41, 1995.

[4] E. Strasser and S. Selberherr, "Algorithms and Models for Cellular Based Topography Simulation," *IEEE Trans.Computer-Aided Design*, 14, 9, 1104–1114, 1995.

[5] A. Myers, J. Doyle, and J. Abelson, "Monte Carlo Simulations of Magnetron Sputtering Particle Transport," *J. Vac. Sci. Technol. A*, 9, 3, 614–618, 1991.

[6] D. N. Ruzic, "The Effects of Surface Roughness Characterized by Fractal Geometry on Sputtering," *Nuclear Instruments and Methods in Physics Research B*, 47, 118–125, 1990.

[7] D. N. Ruzic and H. K. Chiu, "Modelling of Particle-Surface Reflections Including Surface Roughness Characterized by Fractal Geometry," *Journal of Nuclear Materials*, 162-164, 904–909, 1989.